Evolution of wave patterns and temperature field in shock-tube flow

A. D. Kiverin* and I. S. Yakovenko
Joint Institute for High Temperatures, Russian Academy of Science, Izhorskaya 13, Bd. 2, Moscow, 125412, Russia

(Received 26 August 2017; published 29 May 2018)

The paper is devoted to the numerical analysis of wave patterns behind a shock wave propagating in a tube filled with a gaseous mixture. It is shown that the flow inside the boundary layer behind the shock wave is unstable, and the way the instability develops fully corresponds to the solution obtained for the boundary layer over a flat plate. Vortical perturbations inside the boundary layer determine the nonuniformity of the temperature field. In turn, exactly these nonuniformities define the way the ignition kernels arise in the combustible mixture after the reflected shock interaction with the boundary layer. In particular, the temperature nonuniformity determines the spatial limitations of probable ignition kernel position relative to the end wall and side walls of the tube. In the case of low-intensity incident shocks the ignition could start not farther than the point of first interaction between the reflected shock wave and roller vortices formed in the process of boundary layer development. Proposed physical mechanisms are formulated in general terms and can be used for interpretation of the experimental data in any systems with a delayed exothermal reaction start. It is also shown that contact surface thickening occurs due to its interaction with Tollmien-Schlichting waves. This conclusion is of importance for understanding the features of ignition in shock tubes operating in the over-tailored regime.

DOI: 10.1103/PhysRevFluids.3.053201

I. INTRODUCTION

A shock-tube experiment is a common way for studying exothermic reactions in gaseous mixtures. According to the ideal shock-tube theory [1], the induction stage of a thermal explosion proceeds volumetrically at constant temperature and pressure in the mixture compressed by the reflected shock wave. However, this ideal scenario is relevant only to highly reactive mixtures where ignition develops in the so-called "strong ignition" regime. At a lower level of mixture reactivity or relatively low temperature behind the reflected shock, one can observe the "mild ignition" regime. This ignition regime is characterized by the local ignition events proceeding inside spatially separated kernels or even inside a single kernel. For the first time, such an ignition regime was experimentally observed and described by Zaytzev and Soloukhin [2]. Later it was found that "mild ignition" is inherent to most of the experimental techniques including shock tubes operating in the regular regime with two-stage compression [2–6], shock tubes operating in the over-tailored regime with multistage compression [7,8], in flow reactors [9], and in rapid compression machines [10]. As was proposed and vividly demonstrated by Medvedev *et al.* [11], developing of a "mild ignition" scenario is the main reason for differences between kinetic calculations and experimental data at low temperatures. In Ref. [11] it was shown that once locally ignited, the combustible mixture burns down in a deflagration regime faster than autoignition can arise at the ambient temperature. This explanation is corroborated by calculations [11–13] for different mixtures including H_2/O_2, $H_2/CO/O_2$, and C_3H_8/O_2. However, origins of the ignition kernels are still poorly understood. In view of this, the unsolved question about

*alexeykiverin@gmail.com

the origins of the ignition kernels seems to be of importance for the interpretation of shock-tube experimental data and for retrieving combustion kinetics properties from these data.

In the experiments carried out in the rapid compression machine [10], it was observed that microparticles accidentally suspended in the reactive mixture ignited before the gaseous phase. On the one hand, the ignition of the particles can cause the formation of ignition kernels in the mixture. On the other hand, these particles could only mark the position of ignition kernels whose origins, in fact, are fully determined by the evolution of the gas-dynamical flow. Possible gas-dynamical origins of ignition kernels were widely studied numerically [14–17]. The main focus of these papers was on the processes in the region of reflected shock wave interaction with the boundary layer. In particular, recent calculations [16,17] clearly showed that ignition kernels in fuel-air mixtures were forming in the vortical flows separated from the wall after the reflected shock interacted with the boundary layer. However, this mechanism is not suitable for all of the experimental cases. Thus in the case of argon-diluted mixtures, the characteristic time of boundary layer diffusion is fairly long, and therefore there may be no vortices breaking away from the walls into the bulk flow on the timescales of a shock-tube experiment. In this case, the most heated region is the shear zone inside the boundary layer. Therefore one should expect to observe ignition directly inside the boundary layer. Such a regime was obtained in recent experiments [18]. However, it should be noted that in Ref. [18] authors deliberately suspended microparticles in the gaseous mixture. As these particles were able to provide additional local energy release due to friction or due to catalytic reactions on their surfaces, the origins of the ignition kernels are not obvious. Actually, there is always some fraction of the particles inside the shock tube, and therefore it is difficult to figure out what factor plays the leading role: whether it is pure gas dynamics or multiphase dynamics of the gaseous mixture with suspended particles. Besides, the other physical mechanisms may be relevant, such as impurities of the gaseous mixture [19], catalytic reactions on the walls, etc.

Ignition events inside boundary layer region were also observed in the closely related class of problems concerning self-ignition of pressurized fuel ejected into the shock tube filled with air (see, e.g., Refs. [20,21]). This fact proves that the evolution of the boundary layer provides additional conversion of kinetic energy into heat inside boundary region. Therefore it seems promising to study independently the gas-dynamical evolution of the flow and the associated possibilities of ignition kernels' formation in the bulk flow or inside boundary layer region. Recent calculations [22] with the use of a rather rough (from our point of view) technique of boundary layer resolution showed that there is a certain distance from the end wall where the ignition kernel formation inside the boundary layer can be expected with higher probability. We also assumed that any kind of shear flow, whether driven by the wall friction or by nonideal rupture of the diaphragm, should cause the development of temperature perturbations due to kinetic energy dissipation into the heat. This suggestion was confirmed by three-dimensional calculations with no account of boundary layers but with consideration of temperature perturbations introduced by a nonideal diaphragm rupture. It turned out that the pattern of ignition kernel development obtained in Ref. [22] is in good agreement with the experimentally observed patterns (see, e.g., Ref. [13]). Furthermore, the data registered by pressure gauges and ionization probes fit well with results obtained numerically. The ignition gives rise to a combustion wave that propagates through the compressed mixture and finally could cause the detonation onset. When analyzing the experimental data one could observe that on the predetonation stage the combustion does not spread over the whole tube cross section. Therefore it is reasonable to assume that the scenario with the ignition kernel birth and development inside the localized region (e.g., inside boundary layer) is quite natural. Considering the facts mentioned above, we have chosen the detailed analysis of the flow evolution behind the incident shock waves as the main aim of the present work. Our obtained results should provide a clear understanding of gas-dynamical origins of ignition kernels. In addition to the main goal of the work we also carried out numerical simulations of the early stage of ignition to confirm the formulated gas-dynamical mechanisms.

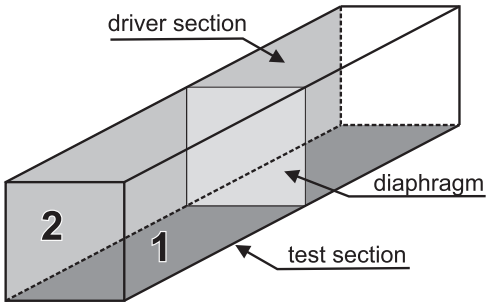

FIG. 1. Schematic diagram of problem setup.

II. PROBLEM SETUP AND NUMERICAL METHOD

Consider a simple problem corresponding to the shock-tube operating regime. Initially two sections of the tube are separated by the infinitely thin diaphragm. One of the sections is filled with the test mixture at low pressure and the second one filled with driver gas at elevated pressure (Fig. 1). The diaphragm ruptures instantly, and the driver gas ejects into the test mixture. According to the classic theory, such discontinuity decay leads to the formation of the shock wave running ahead of the propagating contact surface between the test mixture and driver gas. We chose an argon-diluted mixture of hydrogen with oxygen ($H_2/O_2/Ar$) as a test mixture and helium as a driver gas. The initial parameters of considered test cases are presented in Table I. While carrying out the numerical simulations we were mainly focused on the case of the mild ignition that takes place in hydrogen-oxygen mixtures at temperature lower than so-called crossover value (temperature at which the timescales of the endothermic induction phase and exothermal recombination phase become equal). The reference test mixture composition was the same as in our recent work [22]: 20% ($2H_2 + O_2$) and 80% Ar. The reference temperature behind the reflected shock wave was chosen to be of the order of 900 K, which corresponds to the shock wave speed $D \sim 675\,\mathrm{m/s}$. Also, the cases with $D = 590$–$880\,\mathrm{m/s}$ were considered.

The gas dynamics of the considered processes is governed by the following Navier-Stokes equations written for multicomponent nonreactive gaseous mixture [23]:

$$\frac{\partial \rho}{\partial t} + \frac{\partial \rho u_j}{\partial x_j} = 0, \tag{1}$$

$$\frac{\partial \rho u_i}{\partial t} + \frac{\partial \rho u_i u_j}{\partial x_j} = \frac{\partial \sigma_{ij}}{\partial x_j} - \frac{\partial p}{\partial x_i}, \tag{2}$$

$$\frac{\partial \rho Y_k}{\partial t} + \frac{\partial \rho Y_k u_j}{\partial x_j} = -\frac{\partial \rho Y_k V_{k,j}}{\partial x_j}, \tag{3}$$

$$\frac{\partial \rho E}{\partial t} + \frac{\partial \rho E u_j}{\partial x_j} = \frac{\partial \sigma_{ij} u_j}{\partial x_i} - \frac{\partial p u_i}{\partial x_i} + \frac{\partial}{\partial x_i}\left[\lambda(T)\frac{\partial T}{\partial x_i}\right] - \frac{\partial}{\partial x_j}\left[\rho \sum_k h_k(T) Y_k V_{k,j}\right], \tag{4}$$

$$\sigma_{ij} = \mu(T)\left(\frac{\partial u_i}{\partial x_j} + \frac{\partial u_j}{\partial x_i} - \frac{2}{3}\delta_{ij}\frac{\partial u_l}{\partial x_l}\right), \tag{5}$$

where x_i, spatial coordinates; t, time; ρ, density; p, pressure; T, temperature; u_i, the components of velocity vector; Y_k, the mass fraction of the kth species; E, the specific total energy; σ_{ij}, the viscous stress tensor; $V_{k,j}$, the components of diffusion velocity vector of the kth species; $\lambda(T)$, the mixture-averaged thermal conductivity; $\mu(T)$, the mixture-averaged dynamic viscosity; and h_k, the enthalpy of the kth species. The usual summation convention over repeated indices is assumed. Index k is used to define the type of species as components of the mixture. The values marked with the k index are not involved in the summation over repeated indices. Diffusion velocities are calculated in

TABLE I. Considered test cases.

p_{test}, atm	p_{driver}, atm	D, m/s	2D (Adiabatic wall)	2D (Isothermal wall)	3D	3D (Corner)
			Nonreactive cases			
0.355	1.1	500	+	−	+	−
	2.1	590	+	+	+	+
	3.3	675	+	+	+	+
	8.3	880	+	+	+	+
			Reactive cases			
0.355	3.3	675	+	+	−	−
	4.3	727	−	+	−	−
	5.5	775	−	+	−	−

a zeroth-order Hirschfelder-Curtiss approximation [24], taking into account the correction velocity [25] to ensure mass conservation. Pure species transport coefficients are evaluated utilizing the first principles of gas kinetic theory [26]. Mixture averaged properties are calculated from the pure species parameters with conventional averaging methods [26].

Thermodynamic characteristics of the mixture are related with the use of equations of state written as

$$d(\rho\varepsilon) = C_V(T)dT, \tag{6}$$

$$\frac{p}{\rho} = \frac{RT}{\overline{M}}, \tag{7}$$

where ε, the specific internal energy; $\overline{M} = (\sum_k (Y_k/M_k))^{-1}$, the averaged molar mass; M_k, the molar mass of the kth species, $C_V = C_V(T)$, mixture averaged constant volume specific heat capacity, and R, the universal gas constant. Here heat capacities and enthalpies are calculated using the interpolation of tabulated data [27].

As was mentioned earlier we were mainly focused on the evolution of gas-dynamical flows in the nonreactive medium. However, to confirm the correctness of the proposed gas-dynamical mechanism we carried out additional calculations taking into account chemical reactions. In reactive case Eqs. (3) and (4) were supplied with additional terms $(\frac{\partial Y_k}{\partial t})_{\text{chem}}$ and $\sum_k h_k(T)(\frac{\partial Y_k}{\partial t})_{\text{chem}}$ correspondingly. These terms were calculated using the detailed chemical kinetics mechanism [28].

To achieve high accuracy of the numerical results we used a low dispersive and low dissipative numerical method based on the Compact Accurately Boundary-Adjusting high-Resolution Technique (CABARET) [29]. CABARET is an explicit finite-difference second-order of approximation in space and time scheme with divided calculation of the fluxes and conservative variables that provides unique low-dissipative properties. For solving nonlinear flow problems CABARET uses a flux correction method based on the maximum principle and does not require any parameter tuning or flux limiters. Nonlinear correction ensures accurate balance between dispersion and dissipation errors [29]. This contemporary numerical algorithm has been successfully utilized by its authors [29] to solve a wide range of multiscale unsteady gas-dynamical problems. Here CABARET was adopted to solve reactive and nonreactive multicomponent Navier-Stokes equations with temperature and mixture composition dependencies of transport coefficients and thermophysical properties.

The following boundary conditions were imposed. The closed ends of the tube were solid walls. In the two- (2D) and three-dimensional (3D) case the bottom wall (1 in Fig. 1) was also treated as solid wall while other side walls of the computational domain were symmetry planes. The additional 3D calculations were carried out with two solid walls forming a right angle (1 and 2 in Fig. 1). In Table I and below this case is referred as the "3D (corner)." Accurate resolution of the boundary layer

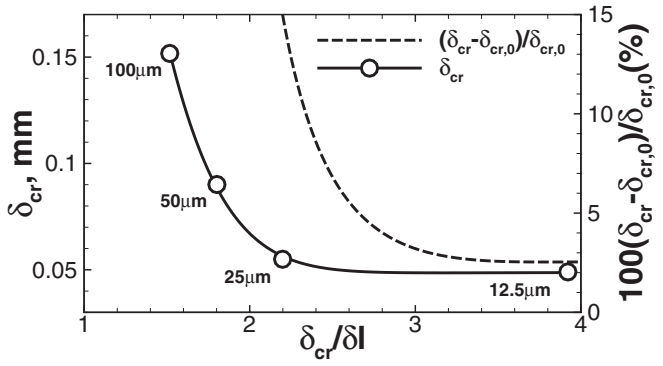

FIG. 2. Convergence test. Dependencies of critical boundary layer thickness and error on the numerical resolution.

development is essential for the considered problem setup. Therefore no-slip boundary conditions were used. The flow velocity at the wall surface was set to zero, and concerning the conditions for temperature we considered two cases: adiabatic and isothermal walls. The adiabatic walls condition allowed us to estimate the rate of kinetic energy dissipation into heat due to the shear flows inside the boundary layer. The case of isothermal walls provided a more realistic estimation of the heating with account of thermal losses to the walls. As will be discussed in detail below, both assumptions provide almost the same gas-dynamical patterns with almost the same characteristic scales. In isothermal case the wall temperature was taken to be equal to the initial temperature of the gas $T_0 = 300\,\mathrm{K}$.

Spatial sizes of the computational domains presented in Fig. 1 were chosen to obtain solution on sufficient spatial timescales. In a 2D setup the lengths of driver section and test section were equal to 0.3 m each. In a 3D setup these lengths were 0.15 m. The transversal length of the domain was 5 mm in the 2D case and 2.5 mm in the 3D case. In the 3D case the length scale in the third dimension was the same as for the transversal one. The considered problem of the boundary layer gas-dynamical instability development is characterized by the following basic parameters: critical boundary layer thickness, Reynolds number calculated for the critical boundary layer thickness, unstable wavelength, and speed of Tollmien-Schlichting waves. However, the critical boundary layer thickness is the main parameter, as all the other parameters are related with it [30]. Due to this fact we carried out a convergence test using the critical boundary layer thickness (δ_{cr}) as a test parameter. Figure 2 represents the results of the convergence test: the dependencies of the δ_{cr} value and error on the numerical resolution of the scale δ_{cr} are shown. The error is estimated relative to the limit value ($\delta_{\mathrm{cr},0}$), which was obtained using the standard routines generally accepted for grid convergence studies:

$$\delta_{\mathrm{cr},0} \approx \delta_{\mathrm{cr},1} - \frac{\delta_{\mathrm{cr},2} - \delta_{\mathrm{cr},1}}{r^k - 1}, \tag{8}$$

where $\delta_{\mathrm{cr},1}, \delta_{\mathrm{cr},2}$, and $\delta_{\mathrm{cr},3}$ are the solutions obtained using the grids with 12.5 μm, 25.0 μm, and 50 μm resolutions, and r is the ratio between cell sizes, which in the considered case was equal to 2.0. The grid convergence order (k) was also obtained as [31]

$$k = \frac{\log\left(\frac{\delta_{\mathrm{cr},2}-\delta_{\mathrm{cr},0}}{\delta_{\mathrm{cr},1}-\delta_{\mathrm{cr},0}}\right)}{\log(r)} = \frac{\log\left(\frac{\delta_{\mathrm{cr},3}-\delta_{\mathrm{cr},0}}{\delta_{\mathrm{cr},2}-\delta_{\mathrm{cr},0}}\right)}{\log(r)}, \tag{9}$$

Using the data presented in Fig. 2 the rate convergence for critical boundary layer thickness was estimated as 2.56. The limit value was estimated as $\delta_{\mathrm{cr},0} = 0.0478\,\mathrm{mm}$. According to this the solution of the particular problem with $\delta l = 12.5\,\mu$m and $\delta l = 25\,\mu$m provided less than 2.5% and 15% errors correspondingly. The results presented in Fig. 2 also clearly show that the formation of

vortical perturbation can be reproduced only with at least 2×2 (in the 2D case) or $2 \times 2 \times 2$ (in the 3D case) computational cells on a vortex scale. For coarser computational cells the solution at small scales was filtered, and only the larger scales of developed instability were resolved. Thus on the coarse grid with $\delta l = 100\,\mu$m only the large-scale perturbations with wavelength not shorter than 0.2 mm were resolved. Therefore the development of gas-dynamical instability started at a farther distance behind the shock front.

Here it is important to note that only the use of the a low-dispersive and low-dissipative numerical method [29] allowed us to obtain such a result. In case of larger numerical dissipation the sufficient level of convergence cannot be achieved at these values of cell sizes δl. Most of the presented results were obtained using $\delta l = 0.025$ mm, and therefore the computational domain consisted of 4.8 million cells in the 2D setup and 120 million cells in the 3D setup. To understand the peculiarities of CABARET usage for reactive flow modeling the reader can refer to the paper [32].

III. RESULTS AND DISCUSSION

Consider the flow forming in the shock tube. The pressurized driver gas expands into the test mixture pushing it towards the closed end of the tube. This leads to the formation of the shock wave propagating ahead of the contact surface in the same direction. The shock wave compresses the test mixture and involves it in the motion behind the shock front. As soon as the shock wave reflects from the end wall the test gas undergoes secondary compression associated with its deceleration behind the reflected shock front. According to the ideal theory of the shock tube exactly these processes are responsible for the reaction start in the test mixture; however, in reality there are always some nonidealities related to the flow evolution.

Let us examine in more detail the behavior of the flow in the multidimensional channel bounded by side walls. In the reference frame attached to the shock front, a control volume of gas passed through the shock front accelerates to velocity $U = U_p - D$, where U_p is the contact surface speed and D is the shock wave speed. Thus in the vicinity of the channel wall, the motion of the compressed test gas is similar to that taking place in the classic problem of the flow over a flat plate. According to the theory [30], such a flow is gas-dynamically unstable. The instability determines the growth of intrinsic perturbations as soon as the boundary layer achieves a certain critical thickness that varies with flow Reynolds number. Criteria for the transition between stable and unstable solutions of this problem are well known and can be found, e.g., in the monograph [30].

Figure 3 illustrates the flow patterns formed inside the boundary layer region behind the shock front for the 2D and 3D cases. For comparison with the solution of flow over a flat plate problem [33–35] we provide a 3D pattern obtained behind the shock front propagating along the planar surface in Figs. 3(c) and 3(d). The visualization, in this case [Figs. 3(c) and 3(d)], allows observing overall evolution of the patterns related to Tollmien-Schlichting waves in the region between the shock wave (1) and contact surface (2), starting with the formation of roller vortices (3), their transformation into the spanwise vortices, and vortices breaking away and formation of the so-called hairpin forest (4). The flow pattern near the corner between two planar surfaces (walls) represents a more complex structure formed due to the interaction between two boundary layers [Fig. 3(e)]. This interaction dictates the faster growth of the boundary layer in the immediate vicinity of the corner and therefore faster transition to the nonlinear phase.

The 2D flow pattern occurs to be less complex but still reproduces all the peculiarities of the flow evolution [Figs. 3(a) and 3(b)]. Moreover, the stage of boundary layer development associated with the formation of roller vortices is also well reproduced in the 2D case. It should be emphasized that exactly this stage determines the origins of ignition kernels, so the flow characteristics defining the formation of ignition kernels are quite close in both the 2D and 3D cases [Fig. 4(a)]. Figure 4(a) shows the numerically obtained dependence between critical boundary layer thickness and the incident shock wave speed. Figure 4(b) shows the relationship between Tollmien-Schlichting wave speed (c_r) normalized by the value of U and the incident shock wave speed D. Besides that, the 2D and 3D solutions considered here correspond well with each other, and they are also in agreement

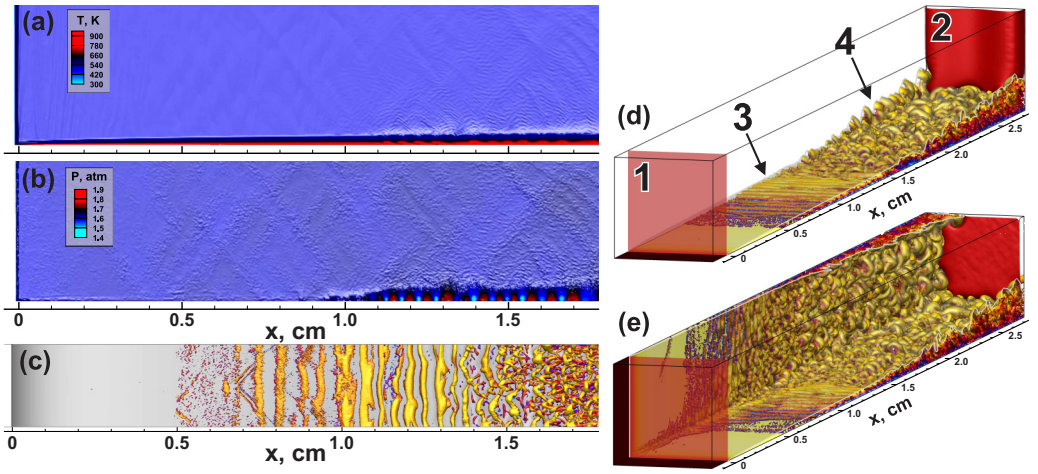

FIG. 3. Flow structure behind the shock wave in 2D channel (a), (b), shock wave propagating along the planar surface (c), (d) and the shock wave in 3D tube of square cross section (e). Panel (a) represents the temperature field, (b) the pressure field. The isosurfaces in (c)–(e) represent the Q criterion value of $Q = 0$. Color in (c)–(e) illustrates the temperature field according to the same palette as in (a). 1, shock front; 2, contact surface; 3, roller vortices; 4, hairpin forest. $x = 0$ corresponds to the shock front position. Case of shock wave speed $D = 675\,\mathrm{m/s}$. The cases with adiabatic boundaries are shown.

with the predictions from linear instability theory. In particular, it is known that according to the linear instability theory c_r could not be higher than $0.42U$, which applies to the considered problem as well. It is obtained that in the case of a D value less than 570 m/s the Tollmien-Schlichting wave speed (c_r) occurs to be higher than $0.42U$ [30], and instability does not evolve [this region is shown in Fig. 4(b) with a dashed line]. The perturbations do not grow, and one does not observe roller vortices formation and their subsequent breakaway. Thus, the results of numerical simulations illustrate clearly that the boundary layer forming behind the incident shock evolves in full accordance with the general laws governing the gas-dynamical flows near the solid surfaces.

To our knowledge the vast majority of studies devoted to the detailed analysis of the flow structures developed on the scales of the boundary layer have been carried out for incompressible gases. However, the analysis of flow patterns obtained in the compressible case shows a relatively good qualitative agreement with the results of incompressible modeling of detached airflows (see, e.g., Ref. [36]). The results obtained in this study also show quantitative agreement with the incompressible case.

Consider in more detail the temperature field developed in the process of the boundary layer evolution. This issue is of paramount importance for understanding the origins of ignition kernels' formation since exactly the temperature nonuniformities define the manner in which chemical reaction would spread in the volume. The boundary layer represents a shear layer where the kinetic energy of the flow dissipates into the heat. This leads to the local temperature rise. Thereby the structure of the unstable boundary layer has a strong impact on the dynamics of the overall process. The growth of perturbations causes the vortices breakaway from the wall and subsequent temperature redistribution inside the heated layer. Thus, one can observe emergence of regions with higher and lower temperature values, compared with the average one. Figures 5(a) and 5(b) illustrate the temperature field forming behind the shock front, while Figs. 5(c) and 5(d) show the temperature profile inside the boundary layer. One can clearly observe nonuniformities in the temperature field inside the region of the developed instability.

Heat losses have a major impact on the temperature field inside the boundary layer. As one can see from the comparison between Figs. 5(a) and 5(b), as well as between Figs. 5(c) and 5(d), the

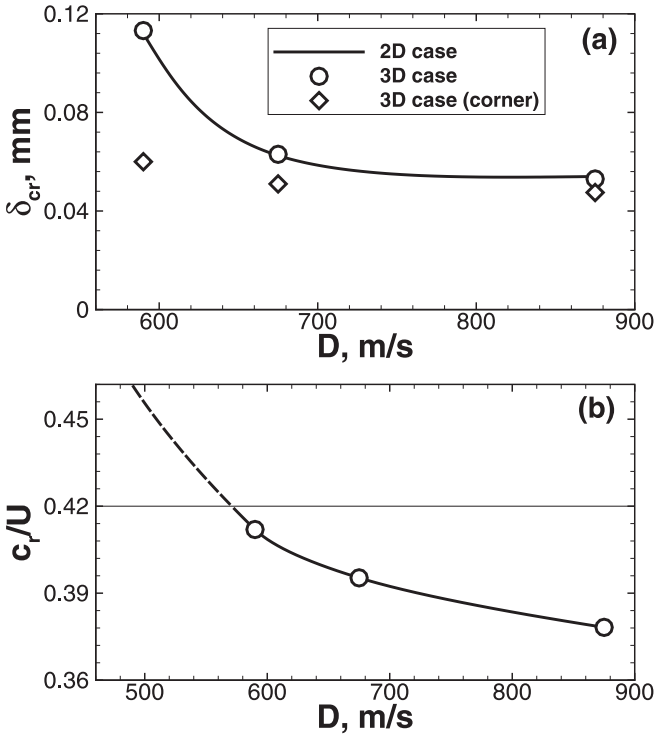

FIG. 4. Dependencies of critical boundary layer thickness (a) and Tollmien-Schlichting wave speed c_r (b) on the incident shock wave speed (D). In panel (b) signs show concrete test cases at different values of D in the unstable region in the 3D case, the dashed line represents solution in the stable region. The 3D case corresponds to the problem setup presented in Fig. 2(d), 3D case (corner) to that in Fig. 2(e).

heat losses through the isothermal wall compensate almost all the energy converted to heat due to the viscous dissipation. And inside the region of instability growth one can see the decrease in temperature even below the value obtained by the shock compression in unconfined space [compare the temperature profiles in Fig. 5(d) with the dashed line representing the temperature value in the ideal case]. Heat transfer to the wall determines the formation of the thermal boundary layer inside which the mean temperature of the flow relaxes to the wall temperature. In the laminar case the thicknesses of viscous and thermal boundary layers are related as square root of the Prandtl number, which is $\sim$0.7 for a wide range of gases. In the case of a developed boundary layer the leading mechanism defining the structures of both boundary layers is related with vortical structures. Due to this fact both boundary layers are characterized by almost the same thickness. Therefore, the interface of the region of the nonuniform temperature field [which can be clearly seen in Figs. 5(a) and 5(b)] correlates well with the boundary layer edge. Since the successful ignition could arise only inside the kernel ("hot spot") of certain spatial size (see, e.g., Ref. [37]) we plot the profiles averaged over the layer of finite thickness Δ [in Figs. 5(c) and 5(d) we chose $\Delta = 0.2$ mm and 1.0 mm].

It is interesting to note that in the considered cases the parameters of gas-dynamical instability, such as critical boundary layer thickness and wavelengths formed in the process of instability development, depend weakly on the temperature values inside the boundary layer (different in cases of adiabatic and isothermal walls). In Fig. 5 one can observe that instability-induced redistribution of temperature arises almost at the same distance behind the shock front independent of the boundary conditions.

After we described in detail the flow patterns developed behind the incident shock wave and related peculiarities of the temperature field, it is useful to analyze the subsequent stage, at which

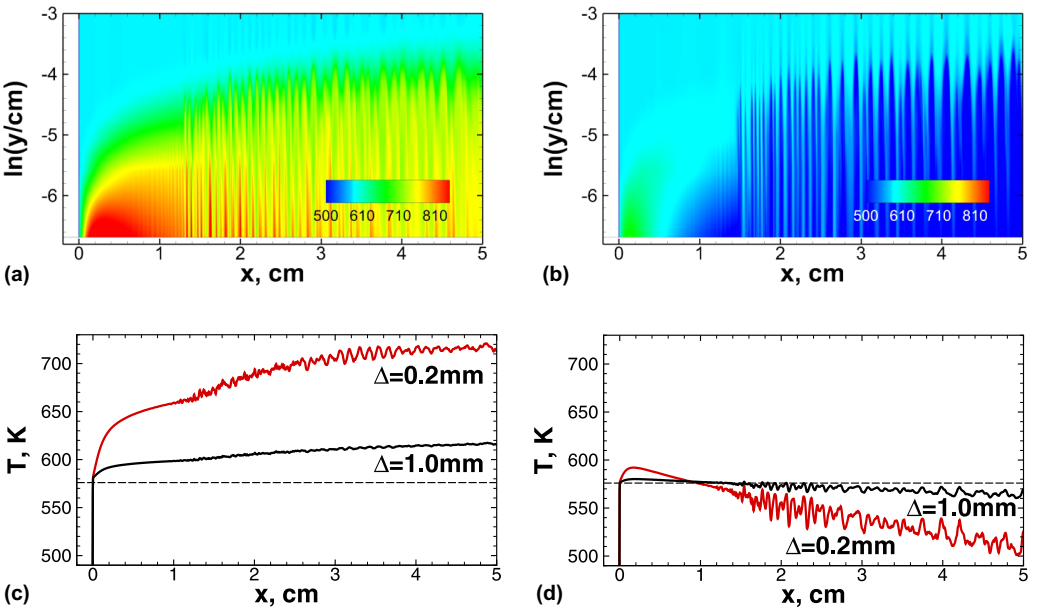

FIG. 5. 2D plots of temperature field (a), (b) and temperature profiles (c), (d) behind the propagating shock at a fixed time instant in the case of adiabatic (a), (c) and isothermal (b), (d) walls. The profiles are averaged over a time interval of 50 μs and over different spatial layers parallel to the wall (values of layer thicknesses are marked as Δ). Dashed line shows the temperature corresponded to the pure shock compression. $x = 0$ corresponds to the shock front position. Case of shock wave speed $D = 675\,\mathrm{m/s}$.

the flow interacts with the reflected shock wave. As the calculations show (see Figs. 3, 5, and 6) the instability arises at the fixed (almost constant) distance behind the shock front ($x \sim 1.2$ cm in the case $D = 675\,\mathrm{m/s}$ or $x \sim 0.7$ cm in the case $D = 727\,\mathrm{m/s}$), in accordance with the classic description of boundary layer instability. The gas involved in the unstable flow continues to move towards the end wall after the shock front reflection and decelerates only after the interaction with the reflected shock. This interaction takes place at a certain distance from the end wall. Numerically obtained visualization of the interaction is shown in Fig. 7. In particular, Fig. 7(a) shows the characteristic

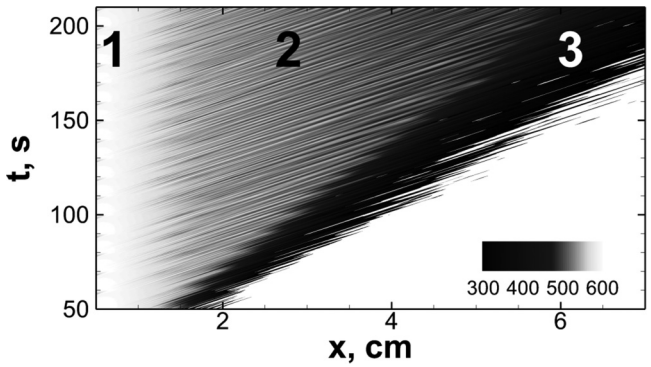

FIG. 6. *x-t* plot of the wave patterns evolving behind the propagating shock. Temperature field is shown in grayscale (see legend). 1, region of stable flow; 2, region of growing instability; 3, broadened contact surface. $x = 0$ corresponds to the shock front position. Case of shock wave speed $D = 675\,\mathrm{m/s}$. Walls are assumed to be isothermal.

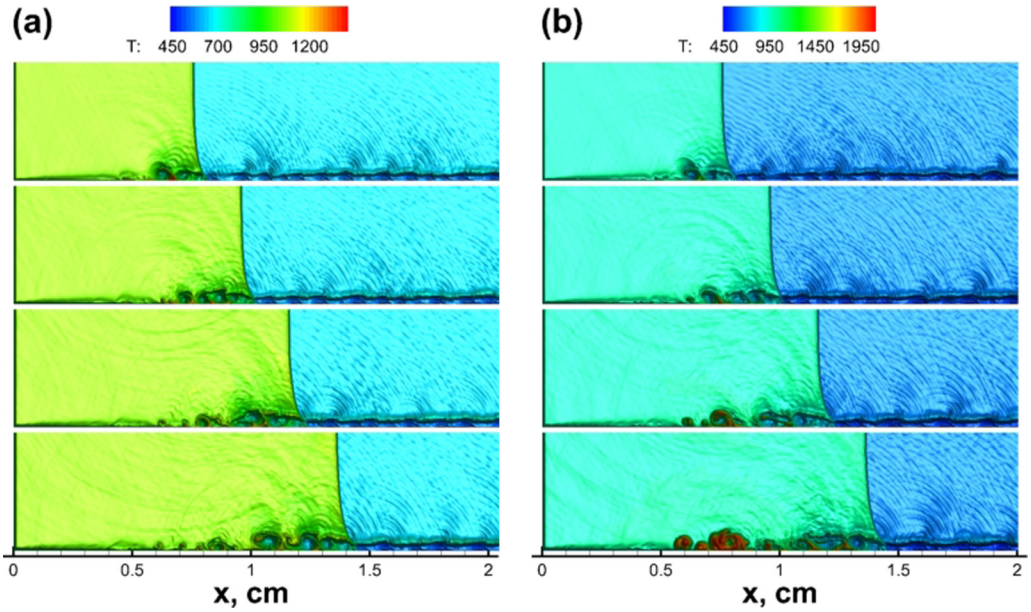

FIG. 7. 2D plots of temperature field in the region of reflected shock interaction with the boundary layer. (a) nonreactive case, (b) reactive case. Shadowgraphy is used to visualize the gas-dynamical perturbations. $x = 0$ corresponds to the end wall. Case of shock wave speed $D = 727$ m/s. Walls are assumed to be isothermal. Time step between frames 5 μs.

temperature field and flow pattern for nonreactive case. One can notice the formation of hot and cold spots inside the boundary layer behind the reflected shock at the distance $x \sim 0.4$ cm from the end wall that corresponds to the position of the first interaction between the reflected shock wave and roller vortices inside the boundary layer. At first, the shock wave interacts with a laminar boundary layer that leads to the shock front bifurcation accompanied by a temperature drop directly behind the shock front. As soon as the shock wave enters the perturbed region the roller vortices are forced to break away from the side wall, transferring temperature perturbations to the area between boundary layer and mean flow. Herein, these perturbations occur to be significantly amplified due to the flow deceleration. In case presented in Fig. 7(a) the temperature inside hot regions associated with the roller vortices separated from the wall achieves up to 1400 K compared with 1045 K in the mean flow. The temperature inside the cold regions directly behind the reflected shock wave drops down to ~900 K. Due to the additional compression of the flow by the reflected shock the formed structures become almost twice as small. Thus, in the case considered in Fig. 7 hot spots formed behind the reflected shock occupy the spatial region of linear size ~0.5 mm, while the characteristic size of roller vortices behind the incident shock wave is ~1.0 mm (close parameters characterize the process in the case $D = 675$ m/s).

Summing up the analysis of the flow patterns behind the reflected shock one can formulate the following conclusions. The nonlinear flow evolution in the region of shock wave interaction with the developed boundary layer leads to the formation of hot spots of finite size (~0.5 mm) and average temperature exceeding the mean value by ~100−200 K. Therefore, the in case of reactive gas most probably the ignition would start exactly inside these hot spots. Such hot spots arise at a a certain distance from the end wall that is fully determined by the peculiarities of boundary layer evolution on the previous stage (behind the incident shock). Hence, the ignition kernels would also be formed at the same distance from the end wall.

To confirm that the proposed gas-dynamical mechanism plays an important role in the formation of ignition kernels, we additionally studied the reactive case. Due to the limitations in computing

resources we were able to study the reactive solution with high enough accuracy only in the 2D case and only at the very early stage of the ignition. However, in the considered case [Fig. 7, $D = 727$ m/s] the ignition delay inside the ignition kernels is rather short, so the observed kernel had enough time to form a stable reaction front on the considered scales [Fig. 7(b)]. Since the ignition kernels are forming immediately after the interaction of the reflected shock with roller vortices region, the 2D solution provides almost the same results as in the 3D case (as was shown above the early stage of boundary layer instability development characterized by the formation of roller vortices is reproduced by the 2D solution with enough accuracy).

Now, let us consider the reacting flow patterns evolved behind the reflected shock after its interaction with roller vortices in the boundary region. As one can clearly see from Figs. 7(a) and 7(b) the deceleration of the vortical flow causes formation of the hot spots immediately after the considered interaction. These hot spots induce the local reaction start. Due to the fact that these initial ignition kernels are associated with the vortices, they could be significantly stretched by the vortical flow that results in reaction quenching. However, these hot regions of partially reacted gas could become the origin of new stable ignition kernels as soon as the corresponding vortex decays. As a result one can observe the formation of the stable reaction front propagating with the speed $\sim$60 m/s from the epicenter in the ignition. The ignition arises directly inside the region of first interaction of the reflected shock wave with the roller vortices. At weaker compression and correspondingly lower mean flow temperature initial ignition kernels quench and are not able to provide successful combustion. In such conditions the ignition starts later at a larger distance from the wall. At stronger compression the ignition takes place at the end wall as is predicted from the ideal shock-tube theory. As well there are some intermediate conditions at which the ignition delay at mean temperature is of the order or a bit longer than the time delay after which the ignition starts at a certain distance from the wall. In such conditions both ignition kernels (weak and strong) could be observed (case $D = 775$ m/s).

It is of certain interest to estimate the quantitative correlation between available experimental data and predictions obtained from the carried out calculations. As can be seen from Fig. 7 in the considered case ($D = 727$ m/s) the successful ignition starts at the distance $\sim$0.7 cm from the end wall. In case of a stronger shock wave ($D = 775$ m/s) the ignition kernel was observed at the distance of 0.5 cm from the end wall. In this case the second kernel directly at the end wall was observed, hence the intermediate conditions mentioned above were acquired. For weaker shock wave ($D = 675$ m/s) we were able to observe only the birth of primary ignition kernel at the distance $\sim$1.0 cm from the end wall (further development of the ignition kernel as well as its stability was limited due to the limitations related with computational resources). For this latter case we also analyzed the experimental data obtained recently in Ref. [22] for close conditions. The experimental data were processed, and the distance of ignition was estimated using gauge readings and general knowledge of the features of detonation development from the ignition kernel [22]. Such an estimation provided us the distance of $\sim$2.0 cm from the end wall. It should be also mentioned that for different hydrogen-containing mixtures ($2\,H_2 + O_2$ [2] and $8\%H_2$ + air [6]) at mean temperature $\sim$900 K similar distances were obtained (1–2 cm [2] and 2–3 cm [6]). In view of this it can be concluded that the obtained numerical results correlate well with available experimental data.

IV. CONCLUSIONS

Our obtained results visualize clearly the flow patterns evolving behind the shock wave propagating inside the tube. One can observe the development of gas-dynamical instability in the boundary layer region. It is interesting to note that the parameters characterizing instability development are in good accordance with those characterizing the instability development in the classic cases such as the flow over a flat plate. The analysis of temperature field associated with the instability development allows explaining the spatial localization of the ignition kernels forming as a result of reflected shock interaction with the flow of the test mixture. On the one hand, the conversion of kinetic energy into heat inside the boundary layer defines the high probability of ignition kernel

formation in the vicinity of the side wall. On the other hand, the developing instability of the boundary layer leads to the spatial limitations of possible distance between the ignition kernel and the tube walls. In the case of less intense incident shocks the ignition can start at some distance from the end wall at the location of interaction between reflected shock wave and roller vortices. Developed instability determines temperature redistribution inside the boundary layer due to the vortices breaking away and subsequent mixing of the heated and partially reacted gas with the cooled one transferred from the side wall. In view of this, it can also be concluded that the most probable region of ignition kernel formation lies near the inner interface between the boundary layer and bulk flow.

It should be noted that it is common to interpret the gas-dynamical processes leading to nonuniformities in temperature field inside chemical reactors heuristically using the terminology of the developed turbulence theory. However, the flow structure at the early stage of gas-dynamical instability development can differ from that at the stage of developed turbulence. Since the temperature field is closely related with the local structure of the flow, it is important to understand at least qualitatively, how the local flow characteristics evolve. The main result of this paper is that the origins of flow nonuniformities in a shock-tube flow are fully determined by the gas-dynamical instability of the boundary layer developed behind the shock wave propagating along the tube surface. As was shown recently in Ref. [38], spatial nonuniformity of the flow along the side wall in the transversal direction restricts the correct interpretation of the shock-tube data. According to the concept proposed in Ref. [38] this nonuniformity could be controlled by the specific side wall profiling. In terms of gas-dynamical instability, this phenomenon can be explained as follows. As has been shown [34], the gas-dynamical instability arises inside the so-called Klebanoff streaks, generally, randomly distributed along the tube surface in the transversal direction. When implementing wall roughness as proposed in Ref. [38] the pattern of flow perturbations becomes more regular. Moreover, the characteristic spatial scales of the wall profile filter the scales of gas-dynamical instability. As a result, one could observe more deterministic flow pattern that should make it easier to interpret the experimental data.

ACKNOWLEDGMENTS

The work was partially funded by President Grant for the state support of young Russian scientists (No. MK-8693.2016.2). The development of the numerical technique and computer codes and the reactive calculations was supported by the Program of the Presidium of Russian Academy of Sciences No. 29, “Fundamental problems of solving the complex practical problems with help of supercomputers.” The research was carried out using the equipment of the shared research facilities of the HPC computing resources at Lomonosov Moscow State University and using supercomputers at the Joint Supercomputer Center of the Russian Academy of Sciences (JSCC RAS).

[1] Ya. B. Zel’dovich and Yu. P. Raiser, *Physics of Shock Waves and High-Temperature Hydrodynamic Phenomena* (Academic Press, New York, 1966).

[2] S. G. Zaytzev and R. I. Soloukhin, Study of combustion of an adiabatically-heated gas mixture, Proc. Symp. (Intern.) on Combust. **8**, 344 (1961).

[3] E. L. Petersen, D. M. Kalitan, A. B. Barrett, S. C. Reehal, J. D. Mertens, D. J. Beerer, R. L. Hack, and V. G. McDonell, New syngas/air ignition data at lower temperature and elevated pressure and comparison to current kinetics models, Combust. Flame **149**, 244 (2007).

[4] R. Blumenthal, K. Fiewege, K. H. Komp, and G. Adomeit, Gas dynamic features of self ignition of non diluted fuel/air mixtures at high pressure, Combust. Sci. Technol. **113**, 137 (1996).

[5] B. E. Gelfand, S. V. Khomik, A. M. Bartenev, S. P. Medvedev, H. Grönig, and H. Olivier, Detonation and deflagration initiation at the focusing of shock waves in combustible gaseous mixture, Shock Waves **10**, 197 (2000).

[6] S. P. Medvedev, Visualization results of hydrogen ignition in shock tubes, in 15th Intl. Symp. Flow Visualization, ISFV15-163-PL7 (2012), http://www.itmo.by/en/conferences/abstracts/isfv_15/.
[7] A. R. Amadio, M. W. Crofton, and E. L. Petersen, Test-time extension behind reflected shock waves using CO_2-He and C_3H_8-He driver mixtures, Shock Waves **16**, 157 (2006).
[8] P. Cadman, G. O. Thomas, and P. Butler, The auto-ignition of propane at intermediate temperatures and high pressures, Phys. Chem. Chem. Phys. **2**, 5411 (2000).
[9] A. Schönborn, P. Sayad, A. A. Konnov, and J. Klingmann, OH*-chemiluminescence during autoignition of hydrogen with air in a pressurised turbulent flow reactor, Int. J. Hydrogen Energy **39**, 12166 (2014).
[10] S. V. Shushkov, T. N. Genarova, V. V. Leshchevich, O. G. Penyazkov, S. V. Gusakova, A. S. Egorov, M. I. Govorov, and Yu. A. Prismotrov, Increase in the rate of fuel combustion on addition of nanosized carbon particles, J. Eng. Phys. Thermophys. **85**, 867 (2012).
[11] S. P. Medvedev, G. L. Agafonov, S. V. Khomik, and B. E. Gelfand, Ignition delay in hydrogen-air and syngas-air mixtures: Experimental data interpretation via flame propagation, Combust. Flame **157**, 1436 (2010).
[12] G. L. Agafonov and A. M. Tereza, Autoignition of propane behind shock waves, Russ. J. Phys. Chem. B **9**, 92 (2015).
[13] V. A. Pavlov and G. Ya. Gerasimov, Measurement of ignition limits and induction times of hydrogen-air mixtures behind the incident shock wave front at low temperatures, J. Eng. Phys. Thermophys. **87**, 1291 (2014).
[14] E. S. Oran, T. R. Young, J. P. Boris, and A. Cohen, Weak and strong ignition: I. Numerical simulations of shock tube experiments, Combust. Flame **48**, 135 (1982).
[15] M. Lamnaouer, A. Kassab, E. Divo, N. Polley, R. Garza-Urquiza, and E. Petersen, A Conjugate axisymmetric model of a high-pressure shock-tube facility, Int. J. Numer. Methods Heat Fluid Flow **24**, 873 (2014).
[16] K. P. Grogan and M. Ihme, Weak and strong ignition of hydrogen/oxygen mixtures in shock-tube systems, Proc. Combust. Inst. **35**, 2181 (2015).
[17] A. Khokhlov, J. Austin, and A. Knisely, Development of hot spots and ignition behind reflected shocks in $2H_2 + O_2$, in the Proceedings of 25th International Colloquium on the Dynamics of Explosions and Reactive Systems (25th ICDERS), UK 0020 (2015), http://www.icders.org/ICDERS2015/.
[18] R. K. Hanson and D. F. Davidson, Advances in shock tube techniques for fundamental studies of combustion kinetics, in the Proceedings of 25th International Colloquium on the Dynamics of Explosions and Reactive Systems (25th ICDERS), UK 0260 (2015), http://www.icders.org/ICDERS2015/.
[19] B. E. Gelfand, S. P. Medvedev, S. V. Khomik, O. E. Popov, A. Y. Kusharin, and G. L. Agafonov, Self-ignition of hydrogen mixtures at high initial pressure, Doklady Akademii Nauk **349**, 482 (1996).
[20] W. Kaneko and K. Ishii, An experimental study on the mechanism of self-ignition of high-pressure hydrogen, Int. J. Hydrogen Energy **41**, 10969 (2016).
[21] M. F. Ivanov, A. D. Kiverin, A. E. Smygalina, V. V. Golub, and S. V. Golovastov, Mechanism of self-ignition of pressurized hydrogen flowing into the channel through rupturing diaphragm, Int. J. Hydrogen Energy **42**, 11902 (2017).
[22] A. V. Drakon, A. D. Kiverin, and I. S. Yakovenko, Temperature perturbations evolution as a possible mechanism of exothermal reaction kernels formation in shock tubes, J. Phys.: Conf. Ser. **774**, 012092 (2016).
[23] K. K. Kuo, *Principles of Combustion* (Wiley, New York, 2005).
[24] J. Hirschfelder, C. Curtiss, and R. B. Bird, *Molecular Theory of Gases and Liquids* (Wiley, New York, 1954).
[25] T. P. Coffee and J. M. Heimerl, Transport algorithms for premixed, laminar steady-state flames, Combust. Flame **43**, 273 (1981).
[26] R. Kee, M. Coltrin, and P. Glarborg, *Chemically Reacting Flow* (Wiley, New York, 2003).
[27] M. W. Chase, Jr., *NIST-JANAF Thermochemical Tables* (American Chemical Society, New York, 1998).
[28] A. Kéromnès, W. K. Metcalfe, K. A. Heufer, N. Donohoe, A. K. Das, C.-J. Sung, J. Herzler, C. Naumann, P. Griebel, O. Mathieu, M. C. Krejci, E. L. Petersen, W. J. Pitz, and H. J. Curran, An experimental and

detailed chemical kinetic modeling study of hydrogen and syngas mixture oxidation at elevated pressures, Combust. Flame **160**, 995 (2013).

[29] S. A. Karabasov and V. M. Goloviznin, Compact accurately boundary-adjusting high-resolution technique for fluid dynamics, J. Comp. Phys. **228**, 7426 (2009).

[30] H. Schlichting, *Entstehung der Turbulenz* (Springer, Berlin, 1959), Sec. 10.

[31] P. J. Roache, Perspective: A method for uniform reporting of grid refinement studies, J. Fluids Eng. **116**, 405 (1994).

[32] M. F. Ivanov, A. D. Kiverin, S. G. Pinevich, and I. S. Yakovenko, Application of dissipation-free numerical method CABARET for solving gasdynamics of combustion and detonation, J. Phys.: Conf. Ser. **754**, 102003 (2016).

[33] X. Wu and P. Moin, Transitional and turbulent boundary layer with heat transfer, Phys. Fluids **22**, 085105 (2010).

[34] T. A. Zaki, From streaks to spots and on to turbulence: Exploring the dynamics of boundary layer transition, Flow Turbul. Comb. **91**, 451 (2013).

[35] G. Eitel-Amor, R. Örlü, P. Schlatter, and O. Flores, Hairpin vortices in turbulent boundary layers, Phys. Fluids **27**, 025108 (2015).

[36] A. D. Beck, T. Bolemann, D. Flad, H. Frank, G. J. Gassner, F. Hindenlang, and C.-D. Munz, Research paper presented at Anade 2013: Advances in numerical and analytical tools for detached flow prediction, Int. J. Numer. Meth. Fluids **76**, 522 (2014).

[37] A. D. Kiverin, D. R. Kassoy, M. F. Ivanov, and M. A. Liberman, Mechanisms of ignition by transient energy deposition: Regimes of combustion wave propagation, Phys. Rev. E **87**, 033015 (2013).

[38] O. Penyazkov and A. Skilandz, Bifurcation parameters of a reflected shock wave in cylindrical channels of different roughnesses, Shock Waves **28**, 299 (2018).